Quasi-elastic processes in ^{58}Ni- and ^{64}Ni-induced reactions on Sn isotopes

A. M. van den Berg,* W. Henning,† L. L. Lee,‡ K. T. Lesko,§ K. E. Rehm, J. P. Schiffer, G. S. F. Stephans,** and F. L. H. Wolfs
Argonne National Laboratory, Argonne, Illinois 60439

W. S. Freeman
Fermi National Accelerator Laboratory, Batavia, Illinois 60510
(Received 22 June 1987)

Quasi-elastic reactions were studied for ^{58}Ni beams at 330 MeV and ^{64}Ni beams at 341 and 380 MeV incident energy, respectively, on even-A Sn isotopes. Angular distributions were measured in the range $20° \leq \theta_{lab} \leq 55°$ using a magnetic spectrograph with a gas-filled focal-plane detector yielding single mass and charge resolution; generally individual states were not resolved. Cross sections for quasi-elastic one-neutron pickup and stripping reactions vary smoothly with the ground-state Q value. Total quasi-elastic transfer cross sections range from 340 to 640 mb, corresponding to 20–40 % of the total reaction cross section determined from the elastic scattering angular distributions. The distribution of the total cross section into the various reaction channels is discussed.

I. INTRODUCTION

The present measurements are part of a systematic study of the distribution of the total reaction strength into various reaction modes in the collision of ^{58,64}Ni beams with targets of even tin isotopes. Previously we had measured fusion followed by particle evaporation[1] and fusion-fission[2] excitation functions for these systems, from energies well below to approximately 1.5 times the Coulomb barrier. From these measurements the strengths and partial-wave distributions of the fusion process were deduced. The results indicate that an appreciable part of the total reaction cross section resides in processes other than compound nucleus formation. Until recently it was believed that, for such a heavy-ion collision at energies above the barrier, the dominant part of this residual strength is found in deep-inelastic processes.

However, recent studies[3,4] of heavy-ion-induced reactions revealed relatively large contributions from quasi-elastic transfer reactions, in particular for the transfer of one or more neutrons. These reactions have angular distributions which peak near the grazing angle. Angle-integrated cross sections for all quasi-elastic neutron transfer reactions have been found to constitute 25% of the total reaction cross section for ^{58}Ni- and ^{48}Ti-induced reactions on ^{208}Pb at bombarding energies of 25% above the Coulomb barrier.[3]

Previous heavy-ion quasi-elastic reaction studies on even-A tin targets[5–8] have mainly focused on a possible enhancement in the cross section for the transfer of one or more neutron pairs coupled to zero angular momentum from one superconducting ground state to another (the "nuclear Josphson effect"). Though some evidence for such enhancement was observed at energies below the Coulomb barrier for Sn-induced[5] and Ni-induced[6,7] reactions on even-A tin isotopes, von Oertzen *et al.*[5] pointed out that at energies well above the Coulomb barrier such effects are less likely to occur because of competition with deep-inelastic processes.

An important quantity for heavy-ion collisions is the total reaction cross section σ_R, which can be derived from a measurement of the elastic scattering angular distributions. However, for most of the systems studied here we did not experimentally resolve the pure elastic scattering from inelastic scattering to low-lying states, which consists partly of Coulomb excitation and partly of nuclear excitation. We will use the term "elastic" to denote the elastic cross sections including the population of low-lying states via inelastic excitation. Therefore, the "reaction" cross section σ_R deduced from this elastic scattering does not include, to first approximation, contributions from Coulomb and nuclear inelastic scattering.

II. EXPERIMENTAL PROCEDURE

Ni beams from the ATLAS accelerator were used in charge state 19^+ with energies of 330 MeV for ^{58}Ni and 341 and 380 MeV for ^{64}Ni, with beam currents of 20–30 e nA on target. Reaction products from collisions of these beams with targets of ^{112,116,120,124}Sn were momentum analyzed with a split-pole spectrograph and measured in a gas-filled position-sensitive focal-plane detection system.[9] The opening angle of the spectrograph was set at 1 msr corresponding to a horizontal angle span of 1.6°. The signals from the two position sensitive wires were used to correct the ΔE signals for path length differences in the detector due to the finite opening angle of the spectrograph. The Z resolution thus obtained in the experiment is typically 0.6 units (FWHM). Targets were made by evaporating isotopically enriched material onto carbon backings. Two sets of targets were used, with thicknesses of 50 and 250 μg/cm^2 with isotopic en-

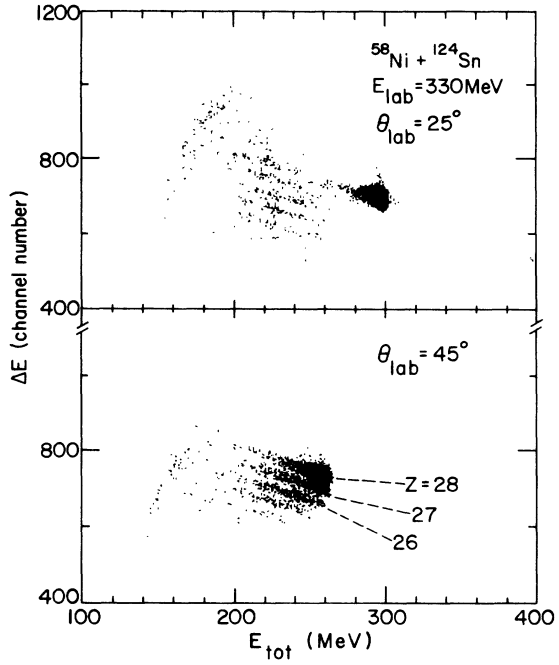

FIG. 1. Scatter plots of ΔE and E_{tot} signals from the spectrograph focal-plane detector for ^{58}Ni + ^{124}Sn at 330 MeV and $\theta_{lab}=25°$ and 45°.

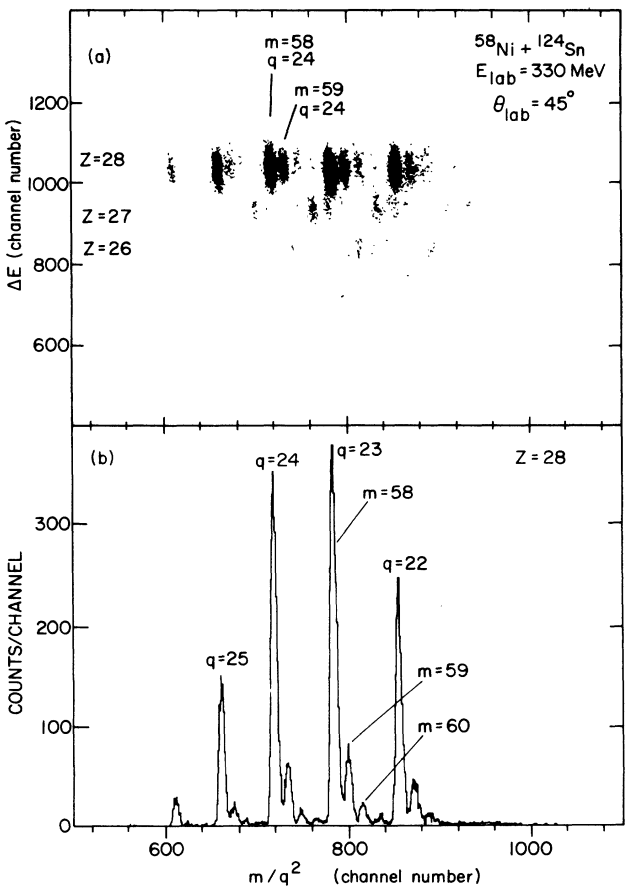

FIG. 2. (a) Scatter plot of ΔE vs $(m/q^2)=(B\rho)^2/E_{tot}$ signals from the spectrograph focal plane detector for the ^{58}Ni + ^{124}Sn reaction at 330 MeV and $\theta_{lab}=45°$. (b) Projection of the scatter plot onto the (m/q^2) axis for $Z=28$.

richment of 80%, 95%, 98%, and 96%, respectively, for ^{112}Sn, ^{116}Sn, ^{120}Sn, and ^{124}Sn. Sn targets have the problem of forming inhomogeneities during the bombardment with heavy ions, and several targets had to be replaced during the run because of this deterioration. The energy resolution was limited by the thickness and the inhomogeneity of the targets. For elastically scattered particles detected at $\theta_{lab}=25°$ the energy resolution ranged from 1.8 MeV for the thin targets to 5 MeV for the thickest targets used.

Figure 1 shows a scatter plot of the corrected ΔE vs total E signals as measured with the focal-plane detector at $\theta_{lab}=25°$ and 45° for ^{58}Ni on ^{124}Sn at 330 MeV. At the forward angles, the yield for the production of elements other than Ni is concentrated at particle energies between 200 and 260 MeV, which is much smaller than the energy for elastically scattered particles (300 MeV at this angle). This process is representative of deep-inelastic scattering. It is seen from Fig. 1 that at the larger angle, on the other hand, the yield for transfer reactions is concentrated at energies comparable to those for elastic scattering, and these processes will be regarded as quasi-elastic reactions. The total energy E and radius of curvature ρ, both measured with the focal-plane detection system, give for each reaction product the yield as a function of the ratio (m/q^2) from which the

TABLE I. Optical model (the potentials are of the Woods-Saxon type) and coupling parameters.

V_0 (MeV)	r_0 (fm)	a (fm)	W (MeV)	r_{0i} (fm)	a_i (fm)	r_C (fm)
100.0	1.25	0.35	40.0	1.25	0.57[a]	1.25

Nucleus	Energy (MeV) $[B(E\lambda)]$ $[(e^2b^\lambda)]$	
	2^+	3^-
^{58}Ni[b]	1.45[0.07]	4.47[0.01]
^{124}Sn[c]	1.13[0.16]	2.61[0.08]

[a]The value of a for the coupled-channels calculation was 0.65 fm; all other parameters were the same.
[b]From Ref. 13.
[c]From Ref. 12.

total yield for the reaction products can be determined by a simple summing (Fig. 2). Differential cross sections were measured in the angular range from 20° to 55°. These cross sections were corrected for charge states which were not detected with the focal-plane detector at a given magnetic field setting; typically these corrections are less than 20%. Relative cross sections were determined from the yield of two fixed monitor detectors at forward angles ($\sim$20°) and the absolute normalization from the yield of elastic scattering measured with the spectrograph at 20° or 25°, by assuming this yield to be purely Rutherford at these angles. We estimate the accuracy of this procedure to be better than 10% for elastic scattering and quasi-elastic neutron transfer cross sections. In the reactions where (quasi-elastic and deep-inelastic) proton transfer is involved, charge-state distribution corrections can be somewhat uncertain due to poor statistics. Estimated errors for these cross sections are 20%.

III. RESULTS

A. Elastic scattering and total reaction cross sections

For the elastic scattering cross section measurements using the 250 μg/cm^2 targets no separation of elastic scattering from low-lying inelastic excitations was possible. For two of the systems, ^{58}Ni + ^{116,124}Sn, measurements with 50 μg/cm^2 targets allowed independent extraction of the pure elastic scattering and inelastic scattering yields. Figures 3 and 4 illustrate the analysis and resulting cross sections for the system ^{58}Ni + ^{124}Sn. The resolution obtained with the thin target was improved to 1.5 MeV by using ray-tracing techniques and by defining a virtual focal plane. The spectra were analyzed using a peak fitting code[10] with the excitation energies for excited states fixed at 1.3 MeV (mean of 2_1^+ states in ^{58}Ni and in ^{124}Sn), 2.6 MeV (mutual 2_1^+ excitation in Ni and Sn and also the 3_1^- state in ^{124}Sn), and 4.5 MeV (the 3_1^- state in ^{58}Ni).

In Fig. 4 we have plotted the resulting angular distributions. The curves are the results from a coupled-channels calculation with the code PTOLEMY,[11] taking into account coupling to the lowest 2^+ and 3^- states in ^{58}Ni and in ^{124}Sn, and to the mutual excitation of the first 2^+ states. The optical model parameters and the coupling constants[12,13] used in the coupled-channels calculations are listed in Table I. Elastic scattering and inelastic cross sections to the first 2^+ states are well reproduced. The predictions of differential cross sections for the yields at excitation energies $E^*=2.6$ and 4.5 MeV are too low, which we attribute to the population of states in this region of excitation which were not taken into account in the calculation (e.g., for ^{58}Ni there are three 2^+ states known around an excitation energy of 3 MeV).

The results for the total reaction cross sections for all systems are summarized in Table II. For the thick target measurements, the reaction cross sections were obtained from optical model fits to the sum of elastic and inelastic cross sections. For the systems ^{58}Ni + ^{116,124}Sn,

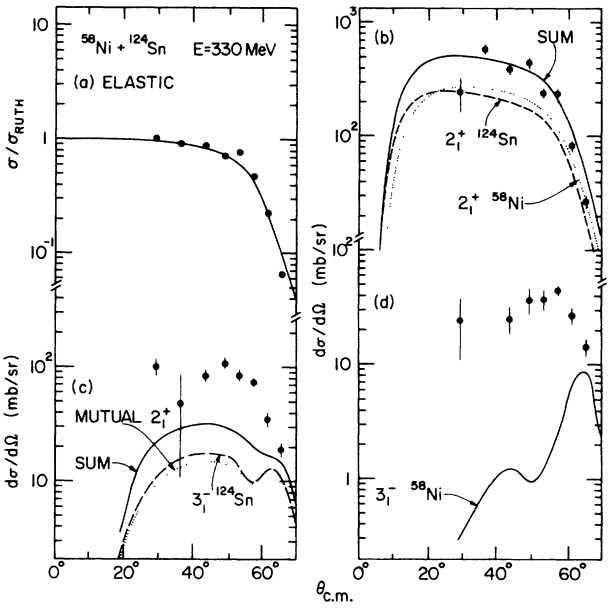

FIG. 3. Differential cross sections for elastic and inelastic scattering for the ^{58}Ni + ^{124}Sn reaction at $E=330$ MeV. Data points are extracted for elastic scattering (a), and for inelastic excitations to states at excitation energies $E^*=1.3$ (b), 2.6 (c), and 4.5 (d) MeV, respectively. Curves are results from coupled channels calculations as described in the text.

where resolved elastic and inelastic yields were analyzed in addition to the thick target yields, good agreement is observed between the total reaction cross sections from the optical model and coupled channels analyses within a 10% uncertainty. This then gives confidence in the reaction cross sections deduced from the thick-target cross sections for the other systems. We have also included in Table II total reaction cross sections obtained within the

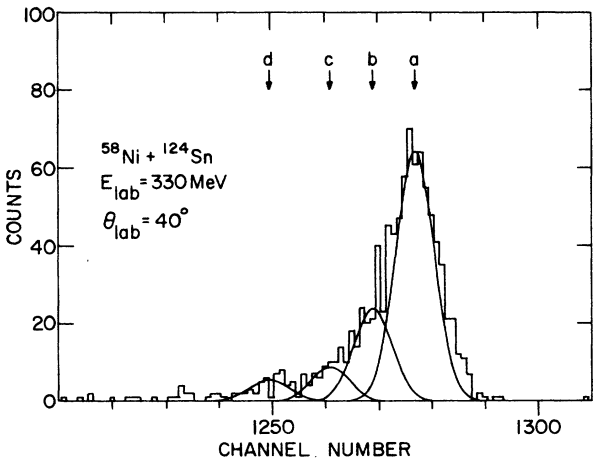

FIG. 4. Magnetic rigidity spectrum for elastic and inelastic scattering yields from the ^{58}Ni + ^{124}Sn reaction at 330 MeV and for the $q=22^+$ charge state. Indicated are positions of the elastic scattering peak (a) and calculated positions for peaks at excitation energies $E^*=1.3$, 2.6, and 4.5 MeV denoted by b, c, and d, respectively.

TABLE II. Total reaction cross sections σ_R for various Ni + Sn systems from the optical model (OM), coupled-channels (CC), and quarter-point ($\theta_{1/4}$) analyses of elastic plus inelastic scattering.

A_t	A_p	E_{beam} (MeV)	$E_{c.m.}$ (MeV)	σ_R (OM) (mb)	σ_R (CC) (mb)	σ_R ($\theta_{1/4}$) (mb)
112	58	330	217	1420		1400
116	58	330	220	1490	1641	1460
120	58	330	223	1470		1560
124	58	330	225	1730	1703	1700
112	64	341	217	1470		1550
116	64	341	220	1530		1610
120	64	341	222	1570		1620
124	64	341	225	1680		1780

diffraction model developed by Frahn[14] from the quarter-point angle $\theta_{1/4}$ of the sum of elastic and inelastic scattering. These values are also consistent with the ones from the optical model fits to better than 10%.

B. Transfer reactions

From Fig. 2 one observes that neutron transfer reactions are the strongest transfer reactions near the grazing angle but that there is also appreciable yield in charge-transfer processes. This is consistent with the systematic behavior of the quasi-elastic processes for Ti-, Ni-, and Si-induced reactions on ^{208}Pb.[3,15] The energy integrated differential cross section can be viewed as consisting of two components. This is illustrated in Fig. 5, which shows angular distributions for the ^{58}Ni-induced one neutron transfer reactions on ^{112}Sn at 330 MeV. These distributions were decomposed into a contribution of Gaussian shape with the peak near the grazing angle, and a contribution falling off exponentially with angle. The Gaussian component gets its main contribution from quasi-elastic reactions ($Q \gtrsim -30$ MeV), while the exponential component is associated with more inelastic processes. A clear distinction between the two processes, however, is not possible. For the Gaussian component, the center-of-mass angles and the Jacobian for the transformation of the laboratory system to the center-of-mass system were calculated assuming zero Q value. This assumption seems justified since the measured optimum Q values are only slightly negative ($Q_{opt} \sim -5$ MeV) for the one-neutron transfer reactions. The angle-integrated cross section σ for the Gaussian component, the centroid θ_m, and the full width at half maximum s, of the angular distributions are listed in Table III for the quasi-elastic neutron-transfer channels.

The cross sections for exchange of one or more protons were summed for each Z without separating the individual masses. The results are shown in Fig. 6. In some cases (e.g., for reactions leading to the production of Cu and Zn isotopes) the quasi-elastic differential cross sections (Gaussian component) were small compared to the deep-inelastic component. For those cases only upper limits for the angle-integrated quasi-elastic cross sections are quoted. Table IV summarizes the contributions from the Gaussian component for the energy- and angle-integrated quasi-elastic transfer cross sections.

IV. DISCUSSION

A. Transfer cross sections

The distribution of the quasi-elastic transfer strength has been discussed in detail in a previous publication.[16] Here, only the main results will be summarized.

(i) The bell-shaped angular distribution for the neutron transfer reactions (Fig. 5), peaked at a center-of-

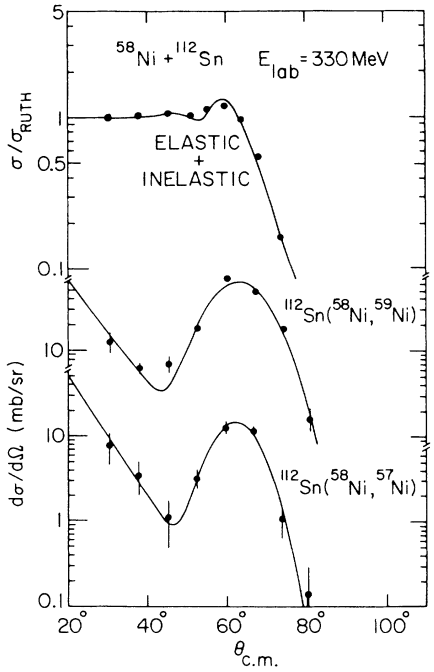

FIG. 5. Angular distributions for the sum of elastic and inelastic scattering and for the neutron transfer reactions ^{112}Sn(^{58}Ni,^{59}Ni)^{111}Sn and ^{112}Sn(^{58}Ni,^{57}Ni)^{113}Sn at a bombarding energy of 330 MeV. The solid line for elastic plus inelastic scattering is the result of an optical model calculation to obtain the reaction cross section. The bell-shaped and exponential curves for the transfer reactions illustrate the quasi-elastic and deep-inelastic contributions, respectively.

TABLE III. Parameters for quasi-elastic neutron transfer reactions ^{A}Sn(^{a}Ni,^{b}Ni)^{B}Sn. (σ is the angle-integrated cross section, and θ_m and s the centroid and full width at half maximum of the Gaussian distribution, respectively. In this analysis, a Q-value cut of $Q \geq -30$ MeV was applied. This condition, however, does not affect the strength of the quasi-elastic cross sections. Uncertainties in s and θ_m are typically $\sim 1°$. The statistical errors in the integrated cross sections are given in parentheses; the overall uncertainty is estimated to be about $\pm 10\%$.)

			2-n stripping			1-n stripping			1-n pickup			2-n pickup		
A	a	E_{beam} (MeV)	σ (mb)	θ_m (deg)	s (deg)	σ (mb)	θ_m (deg)	s (deg)	σ (mb)	θ_m (deg)	s (deg)	σ (mb)	θ_m (deg)	s (deg)
112	58	330	< 10			19(7)	61.3	12	102(5)	61.7	13	34(3)	61.5	16
116	58	330	< 10			19(7)	59.6	14	140(4)	60.1	12	50(2)	60.4	13
120	58	330	< 10			14(5)	57.3	14	156(4)	59.0	12	53(2)	59.2	12
124	58	330	< 10			16(7)	57.3	10	186(4)	57.3	10	52(2)	58.6	10
112	64	341	51(4)	61.0	13	116(6)	61.2	12	62(5)	60.3	13	22(4)	60.0	17
116	64	341	42(5)	59.7	13	103(5)	59.6	11	81(5)	59.2	12	35(24)	50.0	23
120	64	341	29(3)	58.2	11	87(7)	57.8	12	102(6)	57.6	11	18(5)	55.0	13
124	64	341	13(4)	55	14	63(6)	56.4	12	137(7)	55.8	10	34(3)	57.2	11
112	64	380	77(5)	48.5	14	172(8)	50.1	10	82(5)	51.0	9	32(3)	48.2	15
116	64	380	50(4)	49.0	11	172(6)	47.7	11	101(6)	49.3	10	27(3)	47.9	13
120	64	380	37(5)	47.3	11	112(8)	48.1	10	154(13)	46.5	12	35(4)	45.6	14

mass angle θ_m, implies a well-defined internuclear distance D between the two colliding nuclei, at which these processes happen. This distance D for one-neutron transfer reactions is roughly 1 fm larger than the strong absorption radius R_a, observed from the quarter-point angle. The full width at half maximum s, of the angular distributions for these reactions is less than 15° in most cases, which corresponds to a window of 1.5–2 fm in configuration space. Since most of the quasi-elastic charge transfer yield is also concentrated in the same angular range, this implies a highly localized nucleon exchange interaction exhausting most of the elastic flux entering this region. The quasi-elastic reaction channels should therefore have a dominant influence on the average macroscopic scattering potential at these distances.

(ii) The cross section for one-neutron pickup reactions increases as a function of the mass number A of the target nucleus, while that for stripping reactions decreases (see Table III). This reflects the dependence of the cross section on the ground state Q values. One observes a smooth behavior for the cross section ratio $R = (\sigma_p - \sigma_s)/(\sigma_p + \sigma_s)$, with σ_p (σ_s) being the angle-integrated cross section for the quasi-elastic one-neutron pickup (stripping) reaction, plotted versus the difference in ground state Q values for one-neutron pickup (Q_p) and one-neutron stripping (Q_s).

This behavior most likely reflects the dependence on the ground-state to ground-state Q value (Q_{gg}) found by Artukh *et al.*[17] These authors found an exponential dependence on Q_{gg} for the production cross section of

TABLE IV. Angle-integrated quasi-elastic reaction cross sections σ (Gaussian component of the angular distribution) for elements with $24 \leq Z \leq 30$. [Numbers in parentheses give the total (statistical and systematic) error in the last digit(s).]

			σ (mb)							
A_t	A_p	$E_{c.m.}$ (MeV)	$Z=24$	$Z=25$	$Z=26$	$Z=27$	$Z=28$[a]	$Z=29$	$Z=30$	Summed
112	58	217	23(9)	32(9)	53(14)	101(26)	155(18)	10(3)	< 10	370(40)
116	58	220	17(7)	29(8)	100(25)	138(35)	209(25)	14(4)	< 10	510(50)
120	58	223	17(5)	52(13)	98(25)	148(37)	223(23)	< 10	< 10	540(50)
124	58	225	40(10)	60(15)	130(33)	152(38)	254(26)	< 10	< 10	640(60)
112	64	217	< 10	< 10	22(7)	32(10)	251(27)	74(19)	18(5)	400(40)
116	64	220	< 10	4(2)	12(4)	65(21)	261(37)	47(13)	7(2)	400(40)
120	64	222	2(2)	4(2)	30(9)	71(18)	236(26)	32(9)	6(2)	380(30)
124	64	225	< 10	7(2)	19(5)	54(14)	247(27)	14(5)	< 10	340(30)
112	64	242	< 10	< 10	34(21)	46(13)	363(38)	98(30)	20(7)	560(50)
116	64	245	< 10	< 10	40(11)	49(16)	350(36)	72(19)	22(6)	530(40)
120	64	248	< 10	< 10	49(18)	77(24)	338(38)	55(16)	< 10	520(50)

[a]Summed over quasi-elastic neutron-transfer reactions, thus excluding inelastic excitations.

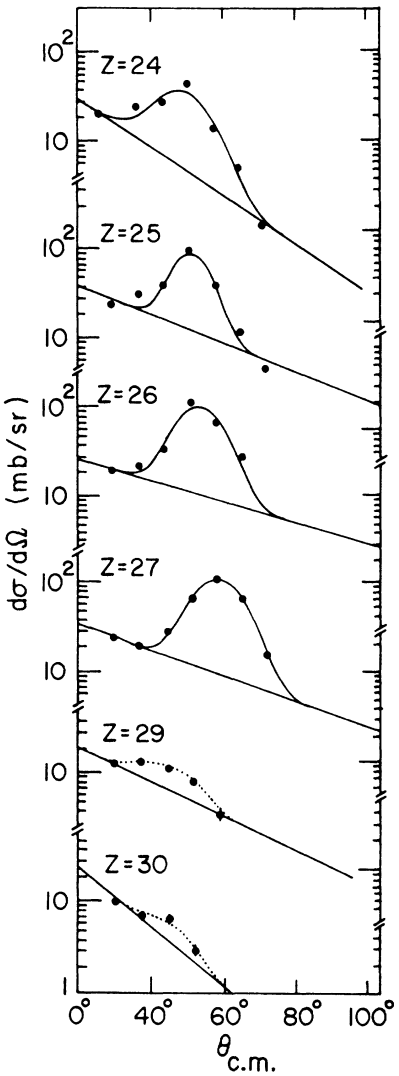

FIG. 6. Angular distributions for Cr ($Z=24$), Mn ($Z=25$), Fe ($Z=26$), Co ($Z=27$), Cu ($Z=29$), and Zn ($Z=30$) isotopes for ^{58}Ni + ^{124}Sn at 330 MeV. The data points represent cross sections integrated over the full excitation energy range. The bell-shaped and exponential curves illustrate the quasi-elastic and deep-inelastic contributions, respectively.

particular species in heavy-ion reactions near the grazing angle. For the cross section ratio R this results in the dependence

$$R=\tanh[\alpha(Q_p-Q_s)/2] ,$$

where α is an adjustable parameter. ($\alpha=0.34$ MeV^{-1}.)

Several authors (among others those of Refs. 18 and 19) have proposed an explanation of the Q_{gg} dependence of Ref. 17 in terms of a statistical process. Abul-Magd *et al.*[19] arrived at the expression for the parameter α:

$$\alpha=[a(A_t+A_p)/(E_{\text{c.m.}}-V_c)]^{1/2} , \quad (4.1)$$

where $a=0.05$ MeV^{-1} is the level density parameter. From the center-of-mass energies for the present systems Eq. (4.1) yields values of α between 0.31 and 0.38 MeV^{-1}, in rather good agreement with the fitted value of 0.34 MeV^{-1}. This good agreement, however, might be fortuitous because the absolute yields for quasi-elastic transfer reactions as a function of the bombarding energy cannot be reproduced by this model.

To reproduce the absolute cross sections as well as the relative yields for proton and multinucleon transfer, there has been some success in parametrizing cross sections along related lines, starting with the work of Ref. 18. This approach takes into account Coulomb effects, and later work also considers the number of nucleons transferred.[20,21] In a similar way we can parametrize our cross sections by

$$\sigma=C\exp[\beta_Q(Q_{gg}+\Delta V_C-Q_{\text{opt}})-\beta_n n-\beta_z z] , \quad (4.2)$$

where ΔV_C is the difference in the Coulomb potentials in the entrance and exit channel, n and z are the number of neutrons and protons transferred, and the optimum Q value Q_{opt} is calculated from Mermaz *et al.*[21] The solid lines in Figs. 7 and 8 are fits of relation (4.2) to the data with four parameters fixed for the whole set of data: normalization constant C, β_Q, β_n, and β_z. The values are given in the captions to Figs. 7 and 8, where the fits to the data are shown.

B. Energy spectra

An important quantity characterizing the nucleon transfer process is the distribution of transfer strength as a function of excitation energy in the final nuclei. In principle, direct-reaction model calculations with a DWBA code such as PTOLEMY (Ref. 11) can be used to predict these energy spectra. However, the large number of final states makes such calculations complicated.

We therefore used the code FAST, based on the diffraction model, to calculate excitation-energy spectra and angle-integrated cross sections for some of the reactions studied here. For the details of such calculations we refer to the papers by Mermaz *et al.*[21] In essence the code FAST folds the density of states populated in the two final nuclei with the transfer cross section calculated with the diffraction model and then calculates the energy spectra for the outgoing particles. The only physically significant parameter is the level density calculated using the particle-hole density function given by Williams,[22] which is constant as a function of excitation energy for one-particle transfer. As examples we show in Fig. 9 energy spectra for ^{57}Ni and ^{59}Ni products for the ^{58}Ni + ^{116}Sn reaction at $E_{\text{lab}}=330$ MeV and $\theta_{\text{lab}}=40°$. The calculated spectra (folded with the experimental energy resolution) are shown as the solid line in this figure.

C. Partial and total reaction cross sections

The data obtained in the present experiment and those from the fusion-fission experiments with the same systems[1,3] allow a partial-wave decomposition of the total reaction cross section into the various reaction modes. To do this, we have performed a DWBA calculation to obtain an approximate l distribution of the quasi-elastic

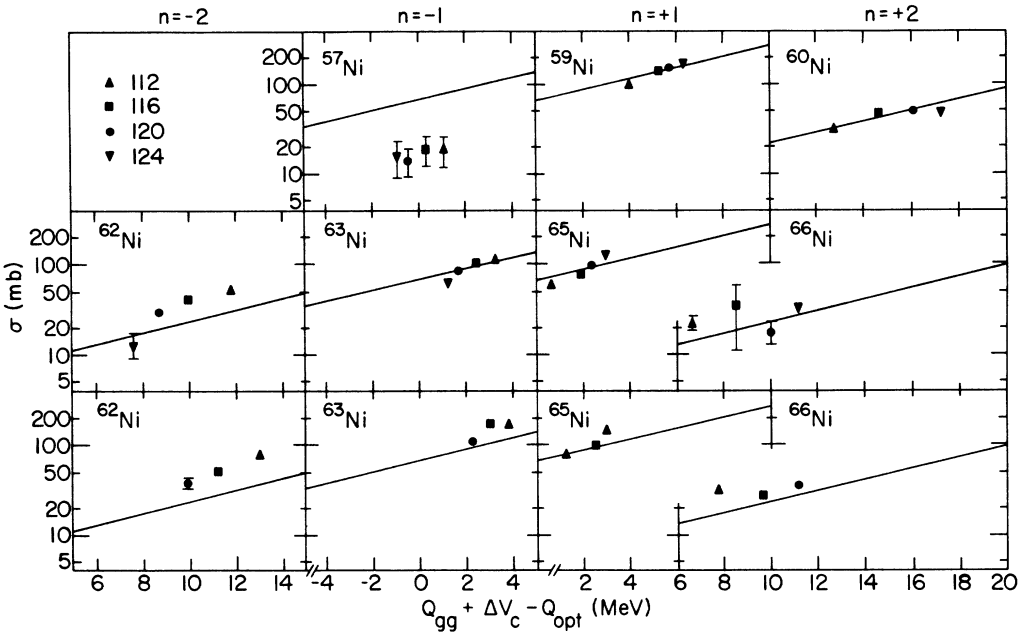

FIG. 7. Quasi-elastic one- and two-neutron transfer reaction cross sections as a function of $(Q_{gg}+\Delta V_C-Q_{\text{opt}})$ for ^{58}Ni- (top) and ^{64}Ni-induced reactions at $E_{\text{lab}}=341$ MeV (middle) and $E_{\text{lab}}=380$ MeV (bottom), respectively. The solid curves are results from fits assuming $\sigma=C\exp[0.14(Q_{gg}+\Delta V_C-Q_{\text{opt}})-2.53n]$ with C constant for all reactions (see the text).

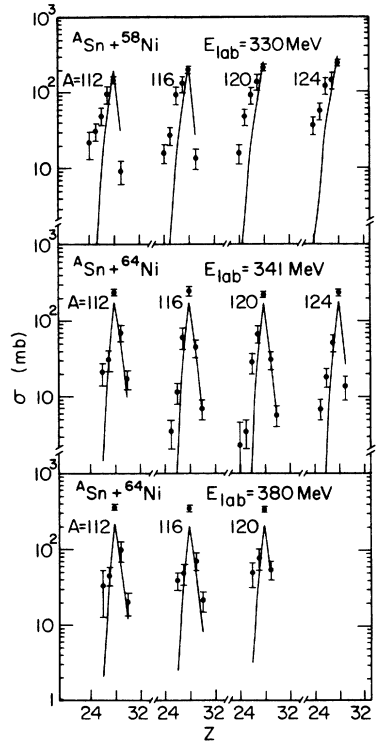

FIG. 8. Quasi-elastic reaction cross sections summed over all isotopes as a function of Z. Errors include systematic errors as discussed in Sec. II. The solid curves indicate calculations for $\sigma=C\exp[0.14(Q_{gg}+\Delta V_C-Q_{\text{opt}})-2.53n-1.61z]$ (see the text).

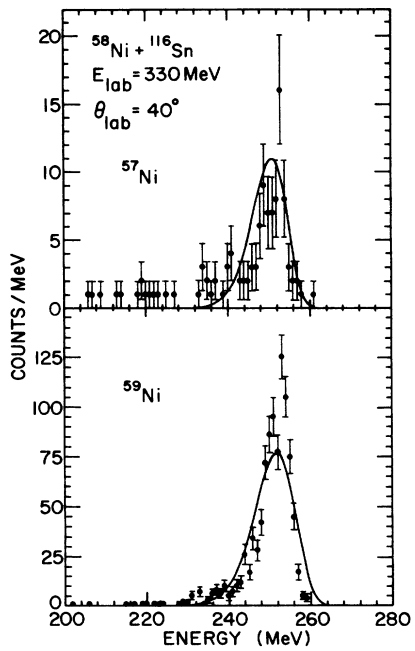

FIG. 9. Measured (error bars) and calculated (solid lines) energy spectra for the ^{116}Sn(^{58}Ni,^{59}Ni)^{115}Sn and ^{116}Sn(^{58}Ni,^{57}Ni)^{119}Sn reactions at $E_{\text{lab}}=330$ MeV and $\theta_{\text{lab}}=40°$. The calculated spectra were generated by the code FAST and folded with the measured energy resolution for elastic scattering. The area under the calculated spectra has been normalized to give the same summed yield as the measurement.

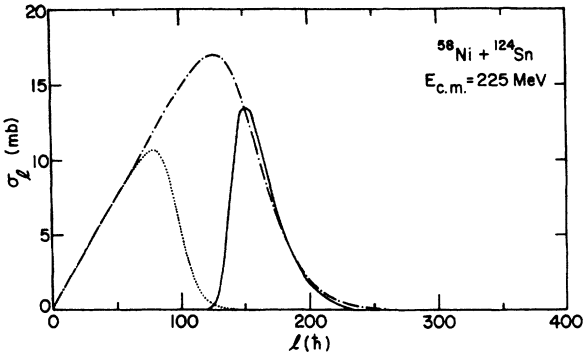

FIG. 10. Decomposition of the reaction cross section for the ^{58}Ni + ^{124}Sn reaction at $E_{c.m.}=225$ MeV. The solid line indicates the partial wave distribution for the total cross section coming from the quasi-elastic reactions. The dotted line gives the distribution for compound nucleus formation as extrapolated from fusion-fission experiments. The dot-dashed line is the result from a CCBA calculation for the total reaction cross section leading to channels other than elastic and inelastic scattering.

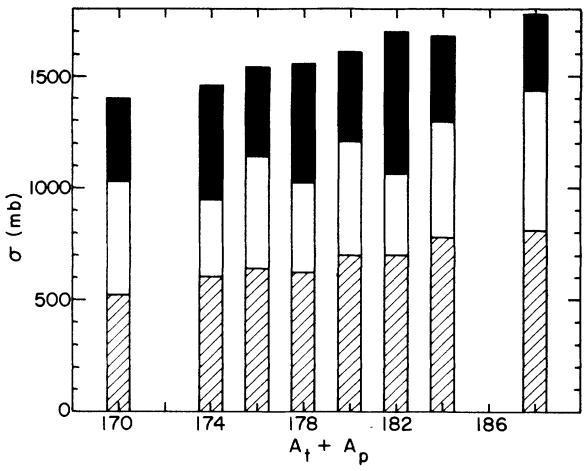

FIG. 11. Decomposition of the reaction cross sections as a function of the total mass number $A_t + A_p$ for the Ni-induced reactions on the even-A Sn isotopes around $E_{c.m.}=220$ MeV. The reaction cross sections and the total quasi-elastic transfer cross section processes (full bars) are from the present study. Shaded bars indicate values for the total fusion cross sections from Refs. 1 and 3. Estimated errors for these cross sections are 100 mb.

transfer strength. In a schematic approach we have calculated the cross section for the one-neutron transfer reaction ^{124}Sn[^{58}Ni,^{59}Ni($\frac{3}{2}^-$)]^{123}Sn($\frac{1}{2}^+$) and then scaled the l distribution to give the total measured quasi-elastic cross section. The result is given as the solid line in Fig. 10. From the fusion-fission experiments between $E_{c.m.}=160$ and 200 MeV (Refs. 1 and 3) we extrapolate the total cross section for compound nucleus formation to be 700 mb at $E_{c.m.}=225$ MeV. From the analysis of the fusion-fission data the diffuseness of the partial wave distribution was found to be $1.5\hbar$, and this number, together with the total fusion cross section, enables us to calculate the partial-wave distribution for compound-nucleus formation (the dotted line in Fig. 10). These partial-wave distributions can now be compared with the results from the coupled-channels Born approximation (CCBA) calculation (dot-dashed curve) discussed in Sec. III A for the total reaction cross section (without inelastic excitations). The partial-wave distribution for the quasi-elastic reactions follows closely the outline of the total reaction cross section. The missing reaction cross section most likely is from deep-inelastic processes and amounts to about 360 mb. Similarly the missing cross sections for other Ni + Sn systems are all of the order of 400 mb and almost independent of the reaction. The decomposition of the reaction cross section into cross sections for compound nucleus formation, deep-inelastic reactions, and quasi-elastic reactions is shown in Fig. 11. It is clear that a measurement of the deep-inelastic reaction cross sections is highly desirable.

V. SUMMARY AND CONCLUSIONS

We have studied quasi-elastic processes for Ni-induced reactions on even-A tin isotopes at beam energies of 330 MeV for ^{58}Ni and 341 and 380 MeV for ^{64}Ni. Total reaction cross sections were obtained from angular distributions for elastic and inelastic scattering. The total cross sections for quasi-elastic neutron transfer reactions are roughly 10–20% of the total reaction cross section. Neutron transfer also forms a constant fraction of the total quasi-elastic transfer cross section: 40% and 65% for ^{58}Ni- and ^{64}Ni-induced reactions, respectively. The yield for the one-neutron pickup and stripping reactions can be explained using a simple parametrized Q-value dependence to represent the available phase space. The systematic trends of the cross section were studied in various systems, which span a factor of 2 in neutron excess. The observed magnitude of the cross sections and their surface localization suggest that quasi-elastic processes play an important role in the average nucleus-nucleus potential, a quantity of considerable interest in near-barrier collisions of heavy systems.

ACKNOWLEDGMENTS

We express our gratitude to the accelerator crew of ATLAS for providing us with ^{58}Ni and ^{64}Ni beams of excellent quality and we wish to acknowledge Dr. S. C. Pieper for his helpful discussions on the CCBA calculations. This work was supported by the U.S. Department of Energy, Nuclear Physics Division, under Contract W-31-109-Eng-38.

*Present address: Fysisch Laboratorium, Rijksuniversiteit Utrecht, 3508-TA Utrecht, The Netherlands.
†Present address: GSI, 6100 Darmstadt, Federal Republic of Germany.
‡Permanent address: State University of New York, Stony Brook, NY 11794.
§Present address: Lawrence Berkeley Laboratory, Berkeley, CA 94720.
**Present address: Massachusetts Institute of Technology, Cambridge, MA 02138.

[1]W. S. Freeman, H. Ernst, D. F. Geesaman, W. Henning, T. J. Humanic, W. Kühn, G. Rosner, J. P. Schiffer, and B. Zeidman, Phys. Rev. Lett. **50**, 1563 (1983).
[2]K. T. Lesko, W. Henning, K. E. Rehm, G. Rosner, J. P. Schiffer, G. S. F. Stephans, B. Zeidman, and W. S. Freeman, Phys. Rev. Lett. **55**, 803 (1985); Phys. Rev. C **34**, 2155 (1986).
[3]K. E. Rehm, D. G. Kovar, W. Kutschera, M. Paul, G. S. F. Stephans, and J. L. Yntema, Phys. Rev. Lett. **51**, 1426 (1983).
[4]A. J. Baltz, P. D. Bond, Ole Hansen, Jiang Cheng-Lie, P. R. Christensen, S. Pontoppidan, F. Videbaek, D. Schüll, Shen Wen-Qing, and H. Freiesleben, Phys. Rev. C **29**, 2392 (1984).
[5]W. von Oertzen, B. Gebauer, H. G. Bohlen, F. Busch, and D. Schüll, Z. Phys. A **313**, 189 (1983).
[6]W. Dünnweber, H. Morinaga, and D. E. Alburger, Phys. Lett. **106B**, 47 (1981).
[7]I. Chiodi, S. Lunardi, M. Morando, C. Signorini, G. Fortuna, W. Starzecki, A. M. Stefanini, G. Korschinek, H. Morinaga, E. Nolte, and W. Schollmeier, Nuovo Cimento **33**, 159 (1982).
[8]S. Pontoppidan, P. R. Christensen, O. Hansen, F. Videbaek, H. C. Britt, B. H. Erkila, Y. Patin, R. H. Stokes, M. P. Webb, R. L. Ferguson, F. Plasil, and G. R. Young, Phys. Rev. C **28**, 2299 (1983).
[9]J. R. Erskine, T. H. Braid, and J. Stoltzfus, Nucl. Instrum. Methods **135**, 67 (1976).
[10]J. R. Comfort, Argonne National Laboratory Physics Division, Informal Report PHY-1970B, 1970; and A. M. van den Berg, Annual Report Kernfysisch Versneller Instituut, 1982, p. 115.
[11]Code PTOLEMY, M. H. Macfarlane and S. G. Pieper, Argonne National Laboratory Report ANL-76-11 (Rev. 1), 1978; M. J. Rhoades-Brown, S. C. Pieper, and M. Macfarlane, Phys. Rev. C **21**, 2417 (1980).
[12]S. Saléem, Vasconcelos, M. N. Rao, N. Ueta, and C. R. Appoloni, Nucl. Phys. **A313**, 333 (1979).
[13]L. K. Peker, Nucl. Data Sheets **42**, 457 (1984).
[14]W. E. Frahn, Nucl. Phys. **A302**, 267 (1978).
[15]J. J. Kolata, K. E. Rehm, D. G. Kovar, G. S. F. Stephans, G. Rosner, and H. Ikezoe, Phys. Rev. C **30**, 125 (1984).
[16]A. M. van den Berg, W. Henning, L. L. Lee, Jr., K. T. Lesko, K. E. Rehm, J. P. Schiffer, J. S. F. Stephans, F. L. H. Wolfs, and W. S. Freeman, Phys. Rev. Lett. **56**, 572 (1986).
[17]A. G. Artukh, V. V. Avdeichikov, J. Erö, G. F. Gridnev, V. L. Mikheev, V. V. Volkov, and J. Wylczynski, Nucl. Phys. **A160**, 511 (1971).
[18]G. B. Bondorf, F. Dickmann, D. H. E. Gross, and P. J. Siemens, J. Phys. Paris C6, Suppl. No. 11–12, **32**, 145 (1971).
[19]A. Y. Abul-Magd, K. El-Abed, and M. El-Nadi, Phys. Lett. **39B**, 166 (1972).
[20]See, for example, J. S. Karp, S. G. Steadman, S. B. Gazes, R. Ledoux, and F. Videback, Phys. Rev. C **25**, 1838 (1982), and references therein.
[21]M. C. Mermaz, R. Dayras, J. Barrette, B. Berthier, D. M. de Castro Rizzo, O. Cisse, R. Legrain, A. Pagano, E. Pollacco, H. Delagrange, W. Mittig, B. Heusch, G. Lanzano, and A. Palmeri, Nucl. Phys. **A441**, 129 (1985), and references therein.
[22]F. C. Williams, Jr., Nucl. Phys. **A166**, 231 (1971).